High-resolution scanning electron microscopy of dopants in p-i-n junctions with quantum wells

Z. Barkay[*], E. Grunbaum[**], Y. Shapira[**], P. Wilshaw[##], K. Barnham[#], D.B. Bushnell[#], N.J. Ekins-Daukes[#], M. Mazzer[#]

*Wolfson Applied Materials Research Centre, Tel-Aviv University, Israel
** Dept. of Physical-Electronics, Faculty of Engineering, Tel-Aviv University, Israel
[##] Dept. of Materials, University of Oxford, UK
[#] Dept. of Physics, Imperial College of Science, Technology and Medicine, London, UK

** Enrique Grunbaum's e-mail for correspondence: enrique@eng.tau.ac.il

ABSTRACT. We have studied the electric field distribution in p-i-n structures with multi-quantum wells (MQW) using the method of dopant (ionization potential) contrast in high resolution (with a cold field emission electron gun) scanning electron microscopy (HRSEM). The samples are GaAs-based ternary compound layer structures used for high-efficiency solar cells, consisting of *p-i-n* junctions, in which various numbers of InGaAs quantum wells have been inserted into the intrinsic (undoped) region. The results show an increasing secondary electron signal across the *n, i* and *p* regions while the series of 8 nm wide quantum wells and their corresponding barriers within the *i*-region are clearly distinguished. The field distribution is obtained by differentiating the dopant contrast curves. This study highlights the capability of HRSEM to provide information on active doping and associated electric fields within electronic nanostructures.

1. INTRODUCTION

The knowledge of dopant concentration and distribution in electron devices is of utmost importance. Amongst several methods of dopant detection and analysis, the observation of secondary electron contrast by high resolution scanning electron microscopy (HRSEM) is promising [1-4]. This signal, which depends partly on doping concentration can be detected with nanometer spatial resolution and needs very simple specimen preparation.

The change in internal energy across a p-n junction, or any junction with different dopant concentrations, gives rise to electrostatic "local (patch) fields" between the differently doped materials due to the redistribution of charge around a p-n junction. It is these electrostatic fields, external to the material, that result in the *n*- and *p*-type material having different ionizations energies, and hence give rise to secondary electron dopant contrast in the HRSEM. It has been shown that the *n*-doped regions produce weaker secondary electron emission (appear darker) than the *p*-type regions and that the secondary electron emission intensity in the *p*-regions is logarithmically proportional to the active dopant concentration [2]. However, if there is significant density of surface states the Fermi level can be pinned mid-gap over a range of relatively low doping concentrations and under these conditions the secondary electron signal, which is actually dependant on the ionization energy, will be independent of the actual doping concentration. It is this effect, which explains why, under some conditions, the doping contrast is insensitive to changes in doping for concentrations lower than ~10^{16}cm^{-3} [2].

2. Experimental

A high-resolution scanning electron microscope with a cold field emission electron gun, providing a highly coherent primary electron beam (JEOL 6700F) has been used, an in-lens secondary electron detector provides an efficient collector. The signal is displayed and measured using a line scan. Contamination of the specimen during observation is reduced to a minimum by using an air lock for its introduction into the UHV microscope chamber. The specimens are a 20-quantum well solar cell and a single-quantum well laser, grown by metallo-organic chemical vapor deposition (MOCVD) at Sheffield University. The layout of their layers is given in Table 1. Cross-sections are prepared by cleavage of the sample very shortly before its introduction into the HRSEM. Observations are made with a primary energy of 2 keV, to reduce the effect of specimen charging, and a primary beam current of 100 pA.

Table 1. Layer layout of the studied samples

Sample QT 1410R			*Sample 432*		
Layer	Thickness nm)	Doping (cm^{-3})	Layer	Thickness (nm)	Doping (cm^{-3})
GaAs	1000	*p* 3x10^{19}	GaAs	400	*p* 2x10^{19}
$Al_{0.8}GaAs$	43	*p*>5x10^{18}	$Al_{0.6}GaAs$	1500	*p* 5x10^{18}
GaAs	200x2	*p* 5x10^{18}			
GaAs	***10***	***i***	***$Al_{0.3}GaAs$***	***250***	***i***
$GaAsP_{0.06}$	***22.7x20***	***i***	***$Al_{0.3}GaAs$***	***70***	***i***
$In_{0,17}GaAs$	***8x20***	***i - QW***	***GaAs***	***10***	***i-QW***
$GaAsP_{0.06}$	***22.7x20***	***i***	***$Al_{0.3}GaAs$***	***70***	***i***
GaAs	***10***	***i***	***$Al_{0.3}GaAs$***	***250***	***i***
GaAs	3000	*n* 2x10^{17}			
GaAs	300	*n* 1.5x10^{18}	$Al_{0.6}GaAs$	1500	*p* 5x10^{18}
GaAs	substrate	n^+	GaAs	substrate	n^+

3. Results and Discussion

Figure 1 shows an increasing secondary electron signal between the *n*, *i* and *p* regions which are clearly distinguished by their different contrast. The secondary electron signal increases at the junction of the n-region with the intrinsic region and extends into the

latter (about 5 QW periods). In the remaining part of the intrinsic region the signal appears to only slightly increase. At the *i/p+* junction there is again a narrow region of a strongly increasing signal.

The band diagram, according to the theory of ionization potential contrast, is drawn in fig. 2. This theory states that the changes in the secondary electron signal correspond to those of the ionization potential, i.e., to changes in the position of the valence band edge. The diagram demonstrates the existence of an electrostatic field due to the built-in potential V_{bi} in the depletion region; the field is strongest at the *n/i* and *i/p* junctions.

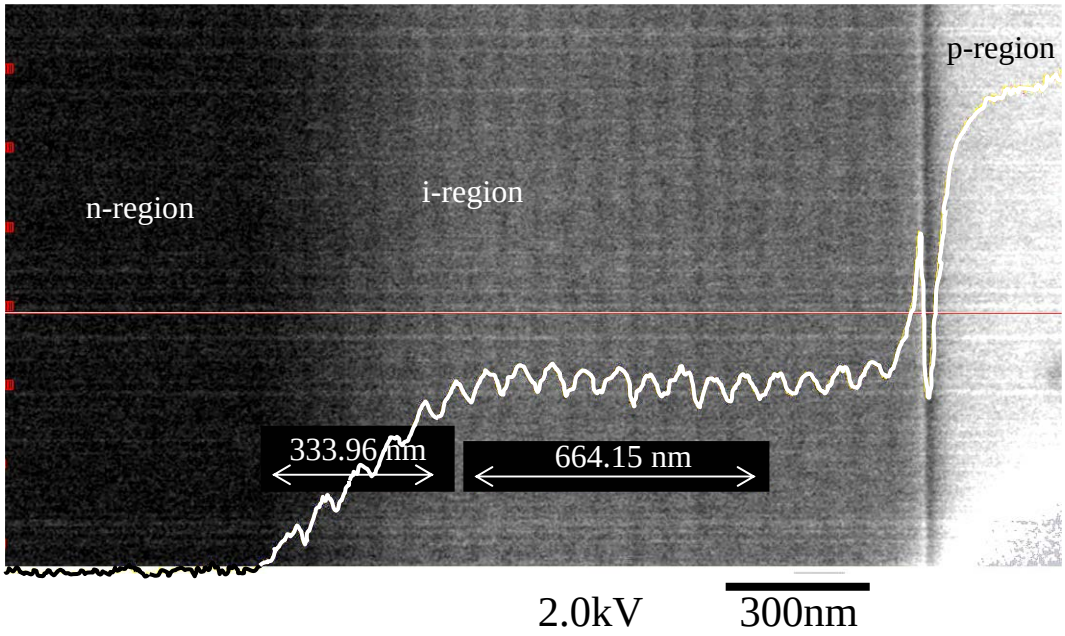

Fig. 1. HRSEM secondary electron line-scan micrograph of sample QT1410R

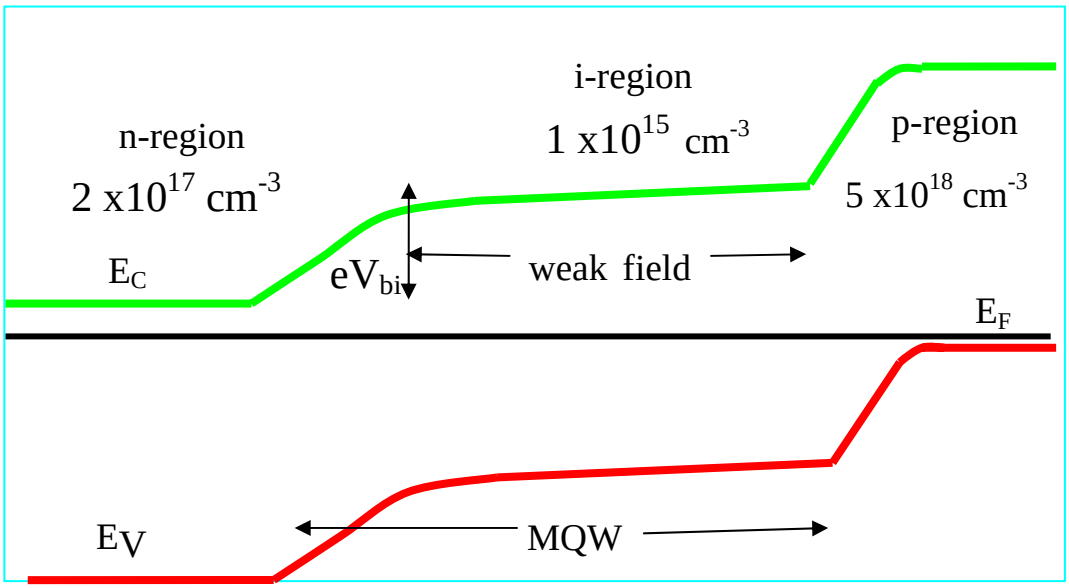

Fig. 2. Proposed band diagram of the *p-i-n* structure

However, for most of the width of the intrinsic region the secondary electron signal is unchanged. This can be explained by a) this being a truly field free region or

alternatively b) by there being a small field present in the bulk layer which is absent at the surface where the doping contrast effect arises. The absence of the field at the surface may be due to the effect of surface states, pinning the Fermi level mid-gap in this region. The latter explanation requires that the doping concentration in this region be lower than a few 10^{16} cm^{-3} and that the bulk field in the intrinsic region is small. This is consistent with measurements of the quantum efficiency (QE) for an applied positive voltage at 0.9 V, which show this to be the case.

The residual doping concentration and its type can be obtained by the measured width of the depletion region (1100 nm) and using equations for abrupt *n-p* junctions [6]: the residual doping is $1x10^{15}cm^{-3}$ (p type) and the built-in potential is 1.2 V. For comparison the HRSEM micrograph of a single QW laser sample (432) is shown (fig. 3). The continuously increasing contrast in the 650 nm wide intrinsic region shows that a strong field exists in the entire region.

In addition to the changes in contrast due to the relatively gradual bending of the valence band produced by the varying doping concentration, abrupt changes can also be seen due to the QWs themselves. This is because the change in semiconductor composition on the nanometer scale associated with these QWs leads to abrupt discontinuities in the valence band edge (and hence ionization potential) which are then imaged in the secondary electron signal.

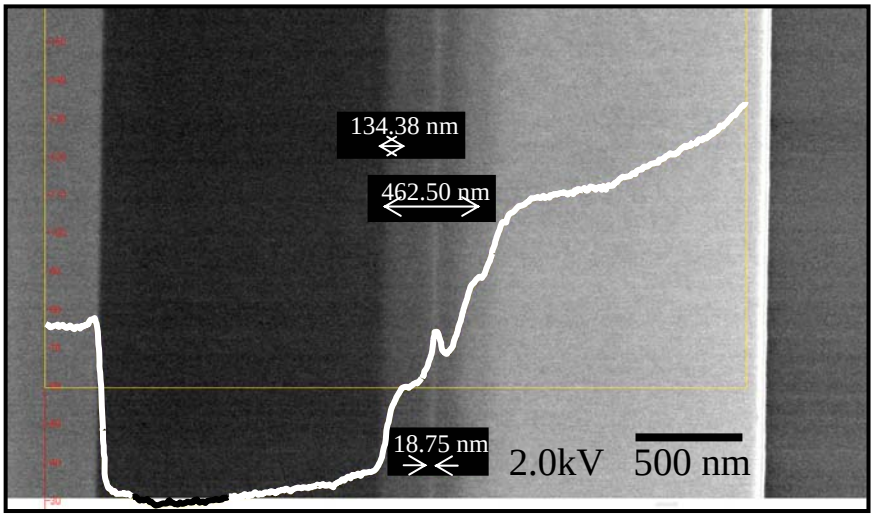

Fig. 3. HRSEM secondary electron line-scan micrograph of sample 432

4. CONCLUSIONS

The results are manifestation of the HRSEM capability to provide useful and easily obtainable information, from a variety of electronic and electro-optical devices, on:
a) The ionization potential and its distribution on a nanometer scale
b) Active dopant concentrations which produce changes in the ionization potential
c) The electric fields due to the built-in potential associated with the dopant distributions.

References

[1] M.R. Castell, D.A. Muller and P.M. Voyles, Nature Materials **2**, 129-131 (2003)
[2] C.P. Sealy, M.R. Castell and P.R. Wilshaw, J. Electron Microsc., **49,** 311 (2000)
[3] S.L. Elliott, R.F. Broom and C.J. Humphreys, J. Appl. Phys., **91**, 9116 (2002)

[4] D. Venables, H. Jain, D.C. Collins, J. Vac. Sci. Tech., **B16**, 262 (1998)
[5] K.W.J. Barnham et al., Physica E**14, 27** (2002)
[6] S.M. Sze, *Physics of Semiconductor Devices*, 2nd ed. (John Wiley, New York, 1981)